Determination of band alignment at two-dimensional MoS_2/Si van der Waals heterojunction

Neeraj Goel, Rahul Kumar, Monu Mishra, Govind Gupta, and Mahesh Kumar

Citation: Journal of Applied Physics **123**, 225301 (2018); doi: 10.1063/1.5030557
View online: https://doi.org/10.1063/1.5030557
View Table of Contents: http://aip.scitation.org/toc/jap/123/22
Published by the American Institute of Physics

Articles you may be interested in

Expansion of a single Shockley stacking fault in a 4H-SiC (11 $\bar{2}$0) epitaxial layer caused by electron beam irradiation
Journal of Applied Physics **123**, 225101 (2018); 10.1063/1.5026448

Optical properties of lonsdaleite silicon nanowires: A promising material for optoelectronic applications
Journal of Applied Physics **123**, 224301 (2018); 10.1063/1.5025856

Reversal time of jump-noise magnetization dynamics in nanomagnets via Monte Carlo simulations
Journal of Applied Physics **123**, 223901 (2018); 10.1063/1.5025691

On matching the anode ring with the magnetic field in an ATON-type Hall effect thruster
Journal of Applied Physics **123**, 223301 (2018); 10.1063/1.5026486

Fast detection and low power hydrogen sensor using edge-oriented vertically aligned 3-D network of MoS_2 flakes at room temperature
Applied Physics Letters **111**, 093102 (2017); 10.1063/1.5000825

High performance NO_2 sensor using MoS_2 nanowires network
Applied Physics Letters **112**, 053502 (2018); 10.1063/1.5019296

PHYSICS TODAY
WHITEPAPERS
MANAGER'S GUIDE
Accelerate R&D with Multiphysics Simulation
READ NOW
PRESENTED BY

JOURNAL OF APPLIED PHYSICS **123**, 225301 (2018)

Determination of band alignment at two-dimensional MoS_2/Si van der Waals heterojunction

Neeraj Goel,[1] Rahul Kumar,[1] Monu Mishra,[2] Govind Gupta,[2] and Mahesh Kumar[1,a)]
[1]*Department of Electrical Engineering, Indian Institute of Technology Jodhpur, Jodhpur 342011, India*
[2]*Advanced Materials and Devices Division, CSIR-National Physical Laboratory (NPL), Dr. K.S. Krishnan Road, New Delhi 110012, India*

(Received 22 March 2018; accepted 23 May 2018; published online 8 June 2018)

To understand the different mechanism occurring at the MoS_2-silicon interface, we have fabricated a MoS_2/Si heterojunction by exfoliating MoS_2 on top of the silicon substrate. Raman spectroscopy and atomic force microscopy (AFM) measurement expose the signature of few-layers in the deposited MoS_2 flake. Herein, the temperature dependence of the energy barrier and carrier density at the MoS_2/Si heterojunction has been extensively investigated. Furthermore, to study band alignment at the MoS_2/Si interface, we have calculated a valence band offset of 0.66 ± 0.17 eV and a conduction band offset of 0.42 ± 0.17 eV using X-ray and Ultraviolet photoelectron spectroscopy. We determined a type-II band alignment at the interface which is very conducive for the transport of photo-excited carriers. As a proof-of-concept application, we extend our analysis of the photovoltaic behavior of the MoS_2/Si heterojunction. This work provides not only a comparative study between MoS_2/p-Si and MoS_2/n-Si heterojunctions but also paves the way to engineer the properties of the interface for the future integration of MoS_2 with silicon. *Published by AIP Publishing.*
https://doi.org/10.1063/1.5030557

I. INTRODUCTION

Two-dimensional (2D) layered materials have opened up new avenues of device miniaturization after scaling-down of devices is no longer possible due to the limitation of silicon.[1–3] However, the limited applications of isolated 2D materials have inspired the researchers to explore van der Waals (vdW) heterojunctions of these 2D layered materials with other materials.[4–6] These vdW heterojunctions become very popular within a short span of time because of their dangling-bond-free surface, tunable properties, and cutting-edge over the conventional semiconductor devices. These heterojunctions also relax the constraints of lattice matching, thus increasing their versatility for various potential applications.[4] Nowadays, MoS_2, being one of the most intensively researched 2D materials, received remarkable consideration for its mixed dimensional heterojunction based applications because of its unique inherited merits including its unconventional mechanical, physical, and structural properties.[7,8] Significant effort has been devoted to integrating MoS_2 with other materials to tune the properties of the interface for desired applications, for instance, light-harvesting and light-emitting devices,[9] high-performance sensors,[10] solar cells,[11] and novel diodes.[5] Gong *et al.*[12] demonstrated a single-step growth strategy for fabrication of seamless and atomically sharp in-plane heterostructures of MoS_2 and WS_2 under different growth temperatures to explore new possibilities of 2D materials. A 2D/3D heterojunction based on the growth of MoS_2 on GaN was reported by Ruzmetov *et al.*[13] to create complex structures for the implementation of high-performance electronic devices.

While earlier reports have explored charge transport at MoS_2 based heterojunctions under photoexcitation,[14,15] the charge transport study under thermal excitation remains elusive. Furthermore, a qualitative comparison between p- and n-type substrates is lacking in the previous reports. Doan *et al.*[16] have investigated the transport properties of the MoS_2/WSe_2 heterojunction via a tuneable charge depletion layer that involves tunneling and recombination. A wide range of MoS_2/Si heterojunction photodetectors with improved attributes has also been actualized.[15,17,18] But most of these reports fail to give a deep understanding of charge transport under thermal excitation. In this study, the impact of temperature on the barrier height and ideality factor of the MoS_2/n-Si heterojunction has been addressed thoroughly. The barrier height can easily be tuned by changing the junction temperature. The increase in temperature results in increasing the thermally induced charge carriers across the interface, which leads to an increase in the on-current. In addition, most of the previous research has focused on monolayer MoS_2 and the hidden potential of few layer MoS_2 (FL-MoS_2) remains unexplored. The monolayer MoS_2 showed a contact resistance and mobility of 740 K $\Omega\,\mu$m and 13 cm^2/V s, respectively, while 5 layer MoS_2 unveils a considerable lower contact resistance and a higher mobility of 1.56 K $\Omega\,\mu$m and 52 cm^2/V s, respectively, with Ti(10 nm)/Au(100 nm) contacts.[19] Kwon *et al.*[20] have also reported a Schottky barrier height as low as 70 meV and a higher mobility of 23.9 cm^2/V s for trilayer thick MoS_2 with Al contacts. Therefore, here we chose FL-MoS_2 because of its lower contact resistance with Au, which results in increasing the on-current and the mobility of the device.

Furthermore, the barrier height and performance of the heterojunction are also strongly dependent on the band

a)Author to whom correspondence should be addressed: mkumar@iitj.ac.in

alignment at the interface.[21,22] To study the band alignment at the MoS_2-silicon heterojunction, we have measured the valence band offset (VBO) and conduction band offset (CBO) values at the heterojunction using X-ray photoelectron spectroscopy (XPS) and Ultraviolet photoelectron spectroscopy (UPS). Depending on the type of band alignment, the hybrid heterojunctions can be utilised for various potential applications, including optoelectronic devices,[23] quantum well structures,[24] and tunnel diodes.[25] Thus, the determination of band offset values and type of band alignment at the MoS_2/Si heterojunction is essential to pave the way for the integration of transition metal dichalcogenides with other materials.

II. EXPERIMENTAL SECTION

We deposited a Si_3N_4 thin layer of 300 nm on the p- and n-type Si substrate having resistivity of 1–10 Ω, using the RF magnetron sputtering technique. A Si_3N_4 target (99.9% purity) was used for thin film deposition in the presence of 45 sccm of Ar and 10 sccm of N_2 at room temperature. RF power applied to the target was 90 W with a chamber pressure of 2.2×10^{-2} mbar. A 200/5 nm thick Au/Cr for making the top contact and a 200 nm thick Al for making the bottom contact were deposited on the Si_3N_4/Si structure by thermal evaporation. Au and Al make an ohmic contact with FL-MoS_2 and n-Si, respectively, while p-Si makes an ohmic contact with Al after annealing the sample for 15 min at $\sim$300 °C in a N_2 ambient atmosphere. A geometric pattern is formed on the Au/Cr/Si_3N_4/Si structure by using UV lithography (Suss MicroTec MJB4) with the help of an optical mask as shown in Fig. 1(a).

The MoS_2/Si heterojunction is formed by mechanically exfoliating MoS_2 from a commercially available crystal of molybdenite (SPI Supplies) using the scotch tape as the transfer medium. The MoS_2 loaded scotch tape is brought into contact with the silicon substrate in order to transfer some of the exfoliated MoS_2 flakes on the silicon. To maximize the contact area between MoS_2 and silicon, the substrate was annealed for 2 min at 100 °C without peeling off the tape. Finally, the stacked heterojunction between MoS_2 and silicon was achieved by removing the scotch tape from the silicon substrate.

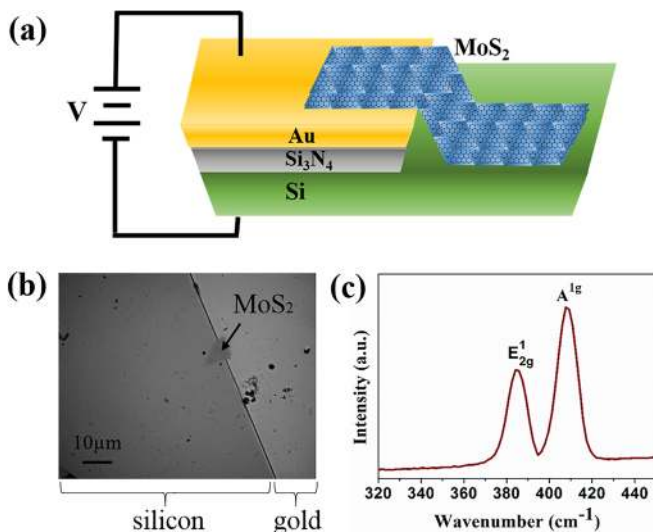

FIG. 1. (a) Three-dimensional schematic diagram of the device. (b) Optical microscopy image taken on the stacked MoS_2/Si heterojunction. (c) Raman spectra of the exfoliated FL-MoS_2 obtained using 514 nm laser excitation.

The thickness of the deposited FL-MoS_2 was confirmed using a Renishaw Raman spectroscopy with a laser excitation wavelength of 514 nm. A park atomic force microscopy (AFM) imaging system was also used to validate the results obtained using Raman spectroscopy. XPS and UPS measurements (Scienta Omicron, Germany) were performed for the calculation of VBO, CBO, and electron affinities at the interface, using an Omicron multiprobe surface analysis system with a monochromatized Al Kα (1486.7 eV) as a radiative source. During the experiment, the MoS_2/Si heterojunction was exposed to 460 nm light irradiation having an intensity of 24 mW cm^{-2}. The electrical characterization was carried out by using a Keithley 4200 semiconductor characterization system.

III. RESULTS AND DISCUSSION

Figures 1(a) and 1(b) show a schematic illustration of the MoS_2/Si heterojunction and an optical micrograph of the FL-MoS_2 deposited on the p-Si substrate with an Au electrode. Raman spectroscopy and AFM measurements have been widely used for studying 2D materials, and mainly for identifying the number of layers. The Raman spectra having peaks of two distinguished vibrational modes E^1_{2g} (in-plane) and A_{1g} (out-of-plane) are located near $\sim$384 and $\sim$408 cm^{-1}, as shown in Fig. 1(c). The difference between the in-plane and out-of-plane vibrational modes is $\sim$24 cm^{-1}, which ensures few-layer behaviour of the exfoliated MoS_2 flakes. Our Raman results are consistent with the earlier reports for the FL-MoS_2 structure.[26] The absolute thickness of exfoliated MoS_2 flakes is further confirmed by using AFM characterization. Figure 2(a) shows the AFM image of FL-MoS_2, and Fig. 2(b) shows the height profile confirming $\sim$3.5 nm of thickness of FL-MoS_2, which is in good agreement with the thickness obtained by Raman spectroscopy. As the mechanically exfoliated MoS_2 cannot be deposited uniformly over all the samples, we made five samples of p- and n-devices each. Out of these ten samples, we choose one sample each of p- and n-type Si having approximately five monolayers ($\sim$3.5 nm) of MoS_2.

Figure 3(a) shows the I-V characteristics of the MoS_2/p-Si heterojunction measured at different temperatures from 100 to 500 K. Au and Al form the ohmic contacts with MoS_2 and p-Si, respectively,[1,27] while the MoS_2/p-Si interface exhibits a rectifying behavior. As we increased the temperature of the device from 100 K to 500 K, the current enhances due to the increment of carrier density at the interface. This increment in the carrier density at the interface of the heterostructure was attributed to thermally generated charge carriers. The current at a temperature of 500 K is approximately 5 times higher than that of 100 K in the MoS_2/p-Si device at 3 V as shown in Fig. 3(a). Moreover, we have also deposited FL-MoS_2 on n-type Si. The I-V characteristics of the MoS_2/n-Si heterostructure are

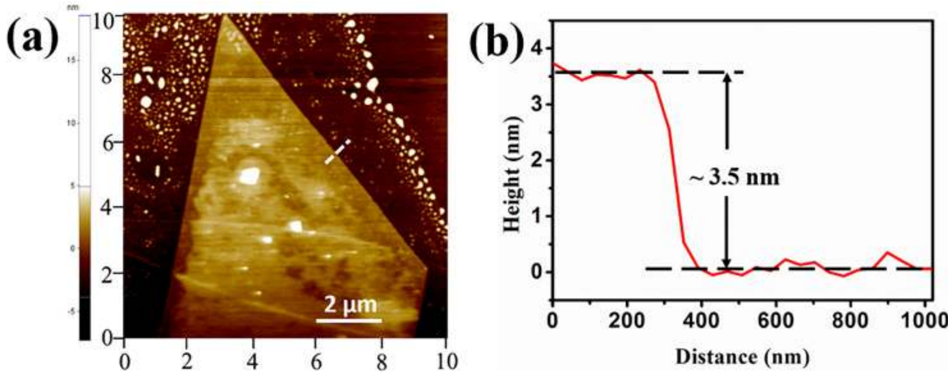

FIG. 2. AFM characterization. (a) AFM image of the exfoliated FL-MoS_2 on Si and (b) the corresponding height profile along the dotted line.

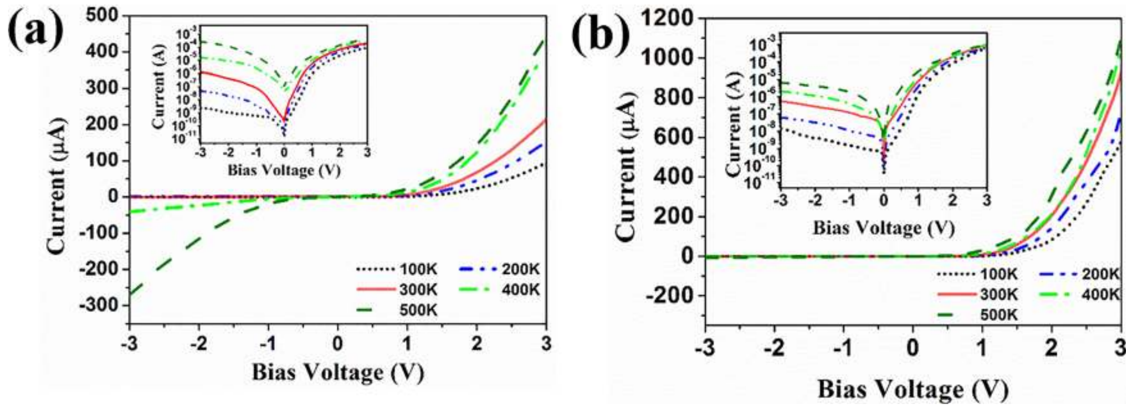

FIG. 3. Current-voltage characteristics measured at different temperatures (100, 200, 300, 400, and 500 K) for (a) the MoS_2/p-Si device and (b) MoS_2/n-Si device. The inset shows current on a log scale.

investigated at different temperatures (T: 100, 200, 300, 400, and 500 K) as depicted in Fig. 3(b), which clearly demonstrates that a barrier is formed at the MoS_2-silicon interface. In the MoS_2/n-Si device, it was found that the current enhances approximately 2 times over a temperature change of 100 K to 500 K at 3 V.

The current flowing across the MoS_2/n-Si heterojunction forming a Schottky barrier at the interface can be approximated by the following standard thermionic emission equation:[28]

$$I = I_0\left[\exp\left(\frac{qV}{\eta k_B T}\right) - 1\right]; \quad I_0 = SA^*T^2\exp\left(-\frac{q\Phi_B}{k_B T}\right), \quad (1)$$

where I_0 is the reverse saturation current, q is the electronic charge, η is the ideality factor, k_B is the Boltzmann's constant, T is the operating temperature, S is the active contact area, A^* is the effective Richardson's constant (112 A cm^{-2} K^{-2} for n-Si),[29] and φ_B is the Schottky barrier height. From Eq. (1), the Schottky barrier height φ_B can be expressed as

$$\varphi_B = \frac{k_B T}{q}\, ln\left(\frac{SA^*T^2}{I_0}\right). \quad (2)$$

The fitting of experimental data shown in Fig. 3(b) to Eq. (1) gives the values of the ideality factor at different temperatures. The ideality factor registered a decrement with an increase in temperature. For the MoS_2/n-Si device, the barrier height which is calculated by using Eq. (1) ranges from 0.185 to 0.780 eV with an increase in temperature (100–500 K). Table I summarizes the various parameters calculated for p- and n-Si devices, including the barrier height, ideality factor, and current density. Table I shows that the barrier height for the n-Si device increases with increasing temperature, which is in contrast to Fig. 3(b). In accordance with Fig. 3(b), current increases with an increase in temperature. These contradictory results indicate that the thermally induced electrons govern the flow of current across the heterojunction and the Schottky barrier height does not play an active role in current conduction.

Bandgap offset values also play a crucial role in modeling heterojunction based electronic and optoelectronic devices.[22] VBO at the MoS_2/p-Si interface can be calculated by using the XPS technique. However, the application of XPS faces two major challenges due to the low escape depth of the emitted electrons. First, to extract electrons from overgrown MoS_2 and the underlying p-Si substrate, the exfoliated

TABLE I. Summary of data taken at different temperatures at the MoS_2-silicon heterojunction.

			J (A/m^2)	
Temperature (K)	Φ_B (eV)	Ideality factor n-Si	p-Si	n-Si
100	0.185	7.3	2.04×10^6	1.39×10^6
200	0.361	4.8	3.25×10^6	2.26×10^6
300	0.522	4.6	4.56×10^6	2.89×10^6
400	0.677	3.8	8.58×10^6	4.09×10^6
500	0.780	2.9	9.63×10^6	4.28×10^6

MoS_2 flake has to be very thin over silicon.[30] The second challenge is a requirement of a large surface area of MoS_2 for XPS measurements.[31] Moreover, because of non-uniformity of MoS_2 over the silicon substrate, the desired area is located by measuring the intensity of Mo 3d and Si 2p core-levels. The method provided by Kraut *et al.*[21] allows us to calculate the precise value of VBO for the MoS_2/Si heterojunction as follows:

$$\Delta E_v = \left(E^{MoS_2}_{Mo3d_{\frac{5}{2}}} - E^{Si}_{Si2p_{\frac{3}{2}}}\right) + \left(E^{Si}_{Si2p_{\frac{3}{2}}} - E^{Si}_{VBM}\right) - \left(E^{MoS_2}_{Mo3d_{\frac{5}{2}}} - E^{MoS_2}_{VBM}\right), \quad (3)$$

where the first term $\left(E^{MoS_2}_{Mo3d_{\frac{5}{2}}} - E^{Si}_{Si2p_{\frac{3}{2}}}\right)$ is the separation in binding energy for Mo 3d and Si 2p core levels of the MoS_2/p-Si interface. The second and third terms are the binding energy difference between the core level and valence band maximum (VBM) of p-Si and MoS_2, respectively. To evaluate VBO at the MoS_2/p-Si interface, we need to calculate the energy of core levels relative to the VBM of MoS_2 and p-Si individually. The VBM positions are calculated by extrapolating the leading edge of VB spectra.[32] The VBM values of 0.91 eV for FL-MoS_2 and 0.2 eV for p-Si were deduced from VB spectra of MoS_2 and p-Si, respectively, as shown in Figs. 4(a) and 4(b). The difference between $Mo3d_{\frac{5}{2}}$ and $Si2p$ core-levels is measured to be 130.17 ± 0.10 eV at the interface [Fig. 4(c)]. Now, the value of $Si2p$ relative to the VBM of Si and the value of $Mo3d_{\frac{5}{2}}$ relative to the VBM of MoS_2 are estimated to be 99.03 ± 0.10 eV and 228.54 ± 0.10 eV, respectively. Thus, the value of VBO is estimated to be 0.66 ± 0.17 eV, by using Eq. (3).

The value of CBO at the MoS_2/p-Si interface can be calculated as follows:

$$\Delta E_c = \Delta E_v + E^{Si}_g - E^{MoS_2}_g . \quad (4)$$

By substituting the values of VBO ($\Delta E_v = 0.66 \pm 0.17$ eV), bandgap of Si ($E^{Si}_g = 1.11$ eV), and MoS_2 ($E^{MoS_2}_g = 1.3$ eV)[18] in Eq. (4), the CBO is measured to be 0.47 ± 0.17 eV. We have also confirmed the calculated value of CBO by using Anderson's affinity rule,[33] by measuring the difference between electron affinities of FL-MoS_2 and Si. In order to calculate electron affinity, UPS measurements of the constituent materials were performed as shown in Figs. 5(a) and 5(b). Electron affinities were determined by using the following relation:[24]

$$\chi = h\nu_{He-I} - W - E_g, \quad (5)$$

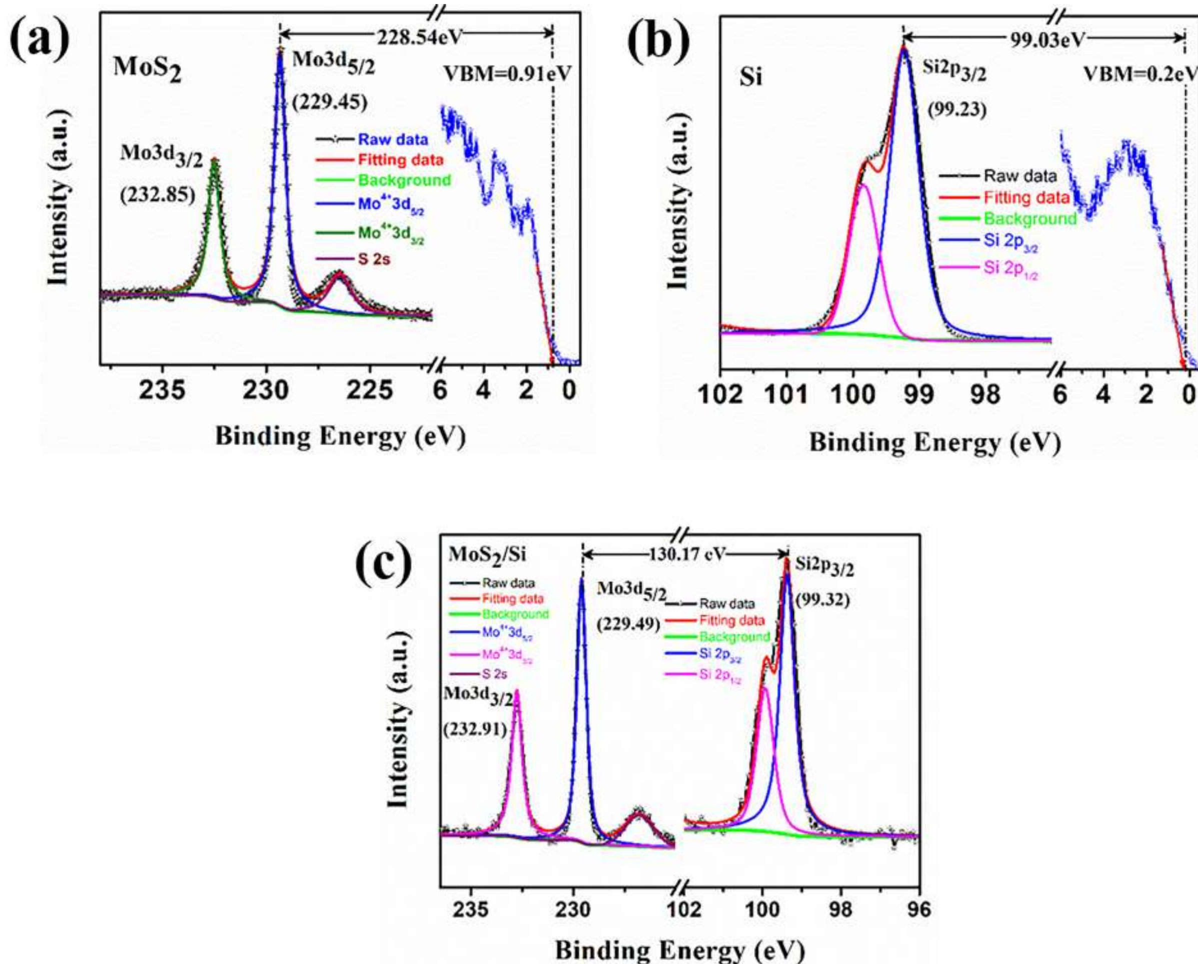

FIG. 4. The x-ray photoelectron spectroscopy (XPS) spectra for (a) isolated MoS_2 flakes, also providing the binding energy separation between Mo 3d core-level and valence band spectra. (b) Si substrate, also representing the binding energy separation between the Si 2p core-level and valence band spectra, and (c) stacked MoS_2/Si heterojunction, showing the binding energy separation between Mo 3d and Si 2p core-levels.

where $h\nu_{He-I}$ is the He-I resonance line photon energy (21.22 eV) emitted from neutral atoms, W is the width of emitted electrons, and E_g is the bandgap of constituent materials. The width of the emitted electrons is calculated by taking into account the difference between the onset of the secondary electrons and VBM as shown in Figs. 5(a) and 5(b). By using Eq. (5), the values of electron affinities were calculated to be 4.32 ± 0.10 and 3.92 ± 0.10 eV for MoS_2 and Si, respectively. Thus, in accordance with the Anderson's affinity rule, CBO is determined to be 0.40 ± 0.10 eV. Our obtained CBO value by using UPS is consistent with that obtained by using XPS [Eq. (3)] within the experimental error bar. Hence, the measured VBO and CBO parameters affirm a type-II band alignment at the MoS_2/p-Si interface as illustrated by the schematic diagram in Fig. 5(c).

Due to the fundamental importance of type-II band alignment in designing flexible optoelectronic devices,[23] we have also explored the optoelectronic relevance and charge-injection mechanism at the MoS_2/Si interface under photoexcitation. In this experiment, a wavelength of 460 nm with the irradiation intensity 24 mW cm^{-2} was used to examine the photovoltaic performance of the MoS_2/Si heterojunction at room temperature. Figures 6(a) and 6(b) depict the I-V characteristics of MoS_2/p-Si and MoS_2/n-Si heterojunctions with and without light irradiation.

At the MoS_2/p-Si heterojunction, a large potential barrier is established due to diffusion of charge carriers at the interface. This potential barrier further increases with an increase in reverse bias. After making contacts between MoS_2 and p-Si, the movement of the Fermi-level at the junction increases the electric field across the interface which separates the electron-hole pairs generated due to light illumination. Thus, the photoinduced current increases due to the increase in carrier density across the interface. Light irradiation not only increases the carrier density but also reduces the barrier height at a reverse biased heterojunction,[34] resulting in an increase of the photocurrent. The reduction in the Schottky barrier height at the MoS_2/n-Si interface by light irradiation can be calculated by using Bardeen's model.[35,36] In this model, the Schottky barrier height decreases linearly with an increase in electric field at the interface, and the reverse current can be expressed as

$$I_0 = I_s\, exp\left(\frac{\beta\sqrt{V_r}}{k_B T}\right), \tag{6}$$

where

$$I_s = S A^* T^2\, exp\left(-\frac{q\Phi r}{k_B T}\right). \tag{7}$$

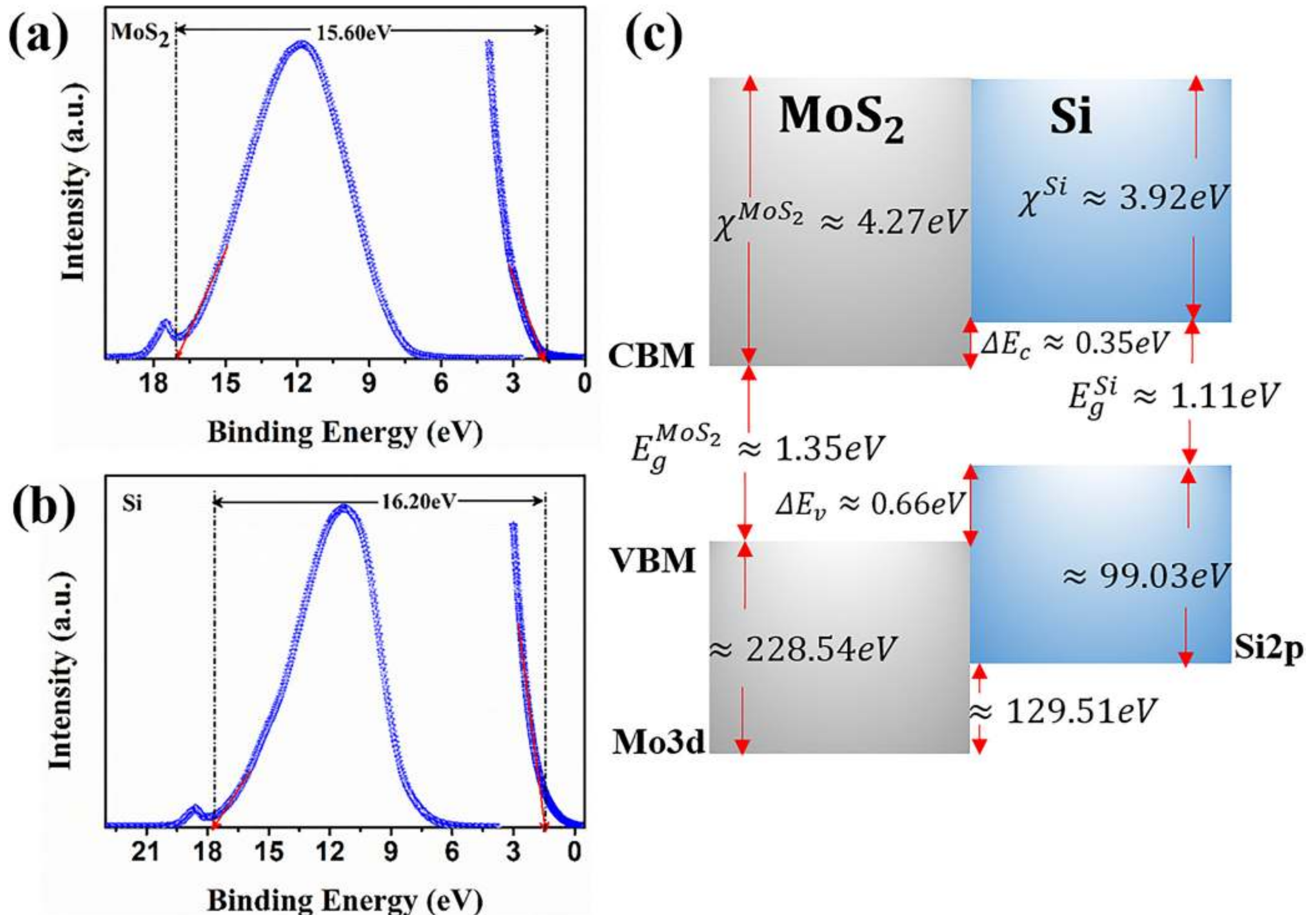

FIG. 5. (a) and (b) Ultraviolet photoelectron spectroscopy (UPS) spectra of the deposited MoS_2 flake and Si substrate. (c) Type-II band alignment schematic representation at the MoS_2/Si heterojunction.

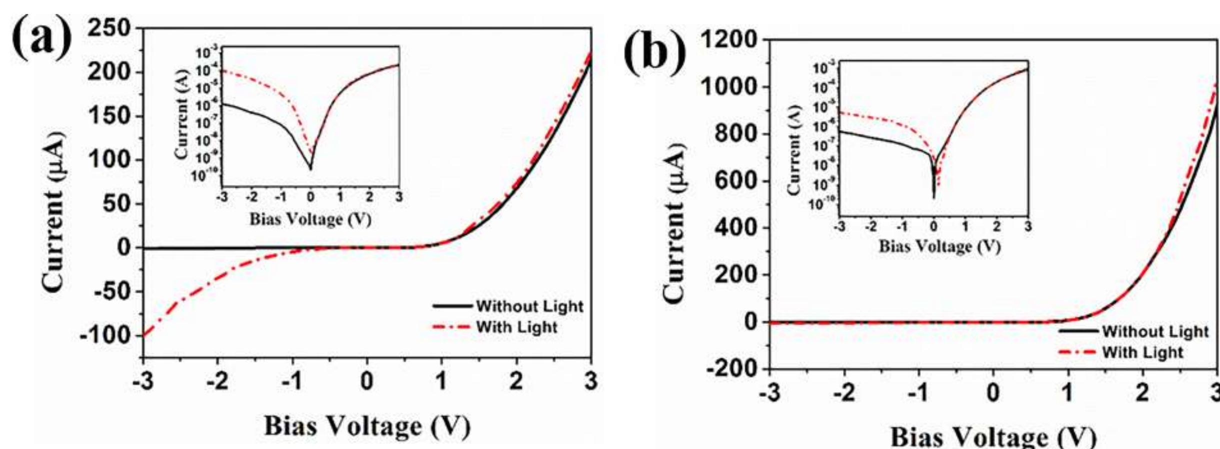

FIG. 6. Current-voltage characteristics of the MoS_2-silicon heterojunction with and without light irradiation: (a) a p-Si device and (b) an n-Si device. The inset shows current on a log scale.

In Eqs. (6) and (7), β is the interface parameter, I_s is reverse saturation current, V_r is the magnitude of applied reverse voltage, T is the operating temperature (300 K), and Φ_r is the reverse barrier height. By fitting of experimental data shown in Fig. 6(b), Eq. (6) yields a reverse Schottky barrier height of 0.522 eV in the dark state and 0.483 eV under 460 nm light irradiation for the MoS_2/n-Si device. Our obtained results are consistent with the earlier reports.[37,38] The dark current and photocurrent are more pronounced in the p-Si device than that of the n-Si device. In the MoS_2/p-Si device, 1.27 μA dark current is observed, which enhances approximately 80 times under 460 nm light irradiation at –3 V. While in the MoS_2/n-Si device, the dark current is only 0.57 μA, which enhances approximately 10 times under light irradiation at –3 V. The Fermi level difference at the interface of MoS_2/p-Si is much lower than that of MoS_2/n-Si, leading to a higher value of dark and photoinduced current in p-Si devices.

IV. CONCLUSIONS

In conclusion, we demonstrated the charge transport studies of the MoS_2-silicon interface under thermal excitation. We observe that the current density at the MoS_2/Si interface increases with an increase in temperature. Moreover, we observed a type-II band alignment at the MoS_2/Si heterojunction which can be used for designing of optoelectronic devices and detectors. As a proof-of-concept application, the photovoltaic behavior of the MoS_2/Si heterojunction was demonstrated for 460 nm light irradiation. This work provides a deep understanding of different mechanisms occurring at the MoS_2/Si interface and opens up new avenues for various 2D/3D integration based applications.

[1]B. Radisavljevic, A. Radenovic, J. Brivio, V. Giacometti, and A. Kis, Nat. Nanotechnol. **6**, 147 (2011).
[2]H. Li, J. Wu, Z. Yin, and H. Zhang, Acc. Chem. Res. **47**, 1067 (2014).
[3]R. Mas-Balleste, C. Gomez-Navarro, J. Gomez-Herrero, and F. Zamora, Nanoscale **3**, 20 (2011).
[4]D. Jariwala, T. J. Marks, and M. C. Hersam, Nat. Mater. **16**(2), 170 (2016).
[5]D. S. Schulman, A. J. Arnold, A. Razavieh, J. Nasr, and S. Das, IEEE Nanotechnol. Mag. **11**, 6 (2017).
[6]S. Srisonphan, ACS Photonics **3**, 1799 (2016).
[7]Y. Yoon, K. Ganapathi, and S. Salahuddin, Nano Lett. **11**, 3768 (2011).
[8]D. Lembke, S. Bertolazzi, and A. Kis, Acc. Chem. Res. **48**, 100 (2015).
[9]P. Li, K. Yuan, D.-Y. Lin, X. Xu, Y. Wang, Y. Wan, H. Yu, K. Zhang, Y. Ye, and L. Dai, Nanoscale **9**(46), 18175 (2017).
[10]R. Kumar, N. Goel, and M. Kumar, ACS Sens. **2**(11), 1744 (2017).
[11]M.-L. Tsai, S.-H. Su, J.-K. Chang, D.-S. Tsai, C.-H. Chen, C.-I. Wu, L.-J. Li, L.-J. Chen, and J.-H. He, ACS Nano **8**, 8317 (2014).
[12]Y. Gong, J. Lin, X. Wang, G. Shi, S. Lei, Z. Lin, X. Zou, G. Ye, R. Vajtai, and B. I. Yakobson, Nat. Mater. **13**, 1135 (2014).
[13]D. Ruzmetov, K. Zhang, G. Stan, B. Kalanyan, G. R. Bhimanapati, S. M. Eichfeld, R. A. Burke, P. B. Shah, T. P. O'Regan, and F. J. Crowne, ACS Nano **10**, 3580 (2016).
[14]Z. Li, J. Chen, R. Dhall, and S. B. Cronin, 2D Mater. **4**, 015004 (2016).
[15]Y. Li, C.-Y. Xu, J.-Y. Wang, and L. Zhen, Sci. Rep. **4**, 7186 (2014).
[16]M.-H. Doan, Y. Jin, S. Adhikari, S. Lee, J. Zhao, S. C. Lim, and Y. H. Lee, ACS Nano **11**, 3832 (2017).
[17]V. Dhyani and S. Das, Sci. Rep. **7**, 44243 (2017).
[18]L. Wang, J. Jie, Z. Shao, Q. Zhang, X. Zhang, Y. Wang, Z. Sun, and S. T. Lee, Adv. Funct. Mater. **25**, 2910 (2015).
[19]W. Liu, J. Kang, W. Cao, D. Sarkar, Y. Khatami, D. Jena, and K. Banerjee, "High-performance few-layer-MoS 2 field-effect-transistor with record low contact-resistance," in *Proceedings of the IEEE International Electron Devices Meeting (IEDM)* (IEEE, 2013), p. 19.4.1.
[20]J. Kwon, J.-Y. Lee, Y.-J. Yu, C.-H. Lee, X. Cui, J. Hone, and G.-H. Lee, Nanoscale **9**, 6151 (2017).
[21]E. Kraut, R. Grant, J. Waldrop, and S. Kowalczyk, Phys. Rev. Lett. **44**, 1620 (1980).
[22]M. Tangi, P. Mishra, C.-C. Tseng, T. K. Ng, M. N. Hedhili, D. H. Anjum, M. S. Alias, N. Wei, L.-J. Li, and B. S. Ooi, ACS Appl. Mater. Interfaces **9**, 9110 (2017).
[23]J. Wang, F. Xu, X. Zhang, W. An, X.-Z. Li, J. Song, W. Ge, G. Tian, J. Lu, and X. Wang, Sci. Rep. **4**, 6521 (2014).
[24]M. Tangi, P. Mishra, M.-Y. Li, M. K. Shakfa, D. H. Anjum, M. N. Hedhili, T. K. Ng, L.-J. Li, and B. S. Ooi, Appl. Phys. Lett. **111**, 092104 (2017).
[25]S. Krishnamoorthy, E. W. Lee, C. H. Lee, Y. Zhang, W. D. McCulloch, J. M. Johnson, J. Hwang, Y. Wu, and S. Rajan, Appl. Phys. Lett. **109**, 183505 (2016).
[26]Y. H. Lee, X. Q. Zhang, W. Zhang, M. T. Chang, C. T. Lin, K. D. Chang, Y. C. Yu, J. T. W. Wang, C. S. Chang, and L. J. Li, Adv. Mater. **24**, 2320 (2012).
[27]B. G. Streetman and S. K. Banerjee, *Solid State Electronic Devices* (Prentice-Hall, 2005).
[28]C. Crowell and S. Sze, Solid-State Electron. **9**, 1035 (1966).

[29]R. Tung, K. Ng, J. Gibson, and A. Levi, Phys. Rev. B **33**, 7077 (1986).
[30]C. S. Fadley, Surf. Interface Anal. **40**, 1579 (2008).
[31]M.-H. Chiu, C. Zhang, H.-W. Shiu, C.-P. Chuu, C.-H. Chen, C.-Y. S. Chang, C.-H. Chen, M.-Y. Chou, C.-K. Shih, and L.-J. Li, Nat. Commun. **6**, 7666 (2015).
[32]T. N. Bhat, M. Kumar, M. K. Rajpalke, B. Roul, S. Krupanidhi, and N. Sinha, J. Appl. Phys. **109**, 123707 (2011).
[33]R. Anderson, IBM J. Res. Dev. **4**, 283 (1960).
[34]J. Liu, P. Fei, J. Song, X. Wang, C. Lao, R. Tummala, and Z. L. Wang, Nano Lett. **8**, 328 (2008).
[35]S. Ranwa, P. K. Kulriya, V. K. Sahu, L. Kukreja, and M. Kumar, Appl. Phys. Lett. **105**, 213103 (2014).
[36]J. Zhang and W. R. Harrell, J. Vac. Sci. Technol. B **21**, 872 (2003).
[37]M.-Y. Lu, M.-P. Lu, S.-J. You, C.-W. Chen, and Y.-J. Wang, Sci. Rep. **5**, 15123 (2015).
[38]M. C. Newton, S. Firth, and P. A. Warburton, Appl. Phys. Lett. **89**, 072104 (2006).